N 62 64637

RM L57L10a

NACA

RESEARCH MEMORANDUM

INVESTIGATION AT TRANSONIC SPEEDS OF A FIXED DIVERGENT EJECTOR INSTALLED IN A SINGLE-ENGINE FIGHTER MODEL

By John M. Swihart and Charles E. Mercer

Langley Aeronautical Laboratory
Langley Field, Va.

NATIONAL ADVISORY COMMITTEE
FOR AERONAUTICS
WASHINGTON

March 3, 1958
Declassified December 8, 1961

NATIONAL ADVISORY COMMITTEE FOR AERONAUTICS

RESEARCH MEMORANDUM

INVESTIGATION AT TRANSONIC SPEEDS OF A FIXED DIVERGENT EJECTOR INSTALLED IN A SINGLE-ENGINE FIGHTER MODEL

By John M. Swihart and Charles E. Mercer

SUMMARY

An investigation of a fixed divergent ejector installed in a single-engine fighter model has been conducted in the Langley 16-foot transonic tunnel. The model was investigated over a Mach number range from 0.80 to 1.07 at zero angle of attack, and the primary-jet total pressure ratio was varied from 1 (jet off) to about 9. A hydrogen peroxide turbojet-engine simulator was used to supply the hot jet exhaust.

The result of the investigation indicated that the jet thrust of a fixed divergent ejector designed for full afterburning operation at a Mach number of 2.0, but operating in the off-design nonafterburning cruise condition with 0.033 corrected secondary-to-primary weight flow ratio, would be about 5 percent less than that of a conical ejector. The static pressure along the divergent walls of the ejector was raised when large quantities of secondary air (14 percent increase in corrected secondary weight flow ratio) were supplied to the ejector. It was found that the external flow field of the model had a significant effect on the base pressures, ejector wall pressures, and the ejector jet thrust.

INTRODUCTION

Several investigations have been conducted at supersonic speeds and at static conditions to determine the efficiency of ejector nozzles in expanding the engine exhaust gases to produce thrust (for example, refs. 1 to 4). It has long been known that a convergent-divergent nozzle develops a high percentage of the ideal isentropic thrust available at design pressure ratio; however, the performance of the nozzle is seriously reduced at pressure ratios below the design condition. (See ref. 5.) Obviously, to maintain peak performance a nozzle having a continuously variable geometry is required. This requirement introduces problems

such as size, weight, and complexity. For these reasons and in spite of the prospect of reduced internal performance at off-design conditions, the fixed divergent ejector may be an attractive type of engine exit configuration because elimination of actuating mechanisms can result in a light and simple structure.

It is the purpose of this paper to show the internal performance characteristics at transonic speeds of a fixed divergent ejector installed in a single-engine fighter model. This represents an off-design condition (nonafterburning cruise operation) for an ejector which was designed for full afterburning operation at a Mach number of 2.0. This investigation was conducted in the Langley 16-foot transonic tunnel at Mach numbers from 0.80 to 1.07 at zero angle of attack. The ejector was installed in a single-engine fighter model described in reference 6. A hydrogen peroxide turbojet-engine simulator of the type described in reference 7 was used to supply the hot jet exhaust. The primary jet total pressure ratio was varied from 1 (jet off) to 5 at all Mach numbers and up to about 9 at all Mach numbers above 1.00.

SYMBOLS

A area, sq ft

AR aspect ratio

C_d discharge coefficient, $\frac{w_p}{w_{p,i}}$

C_p pressure coefficient, $\frac{p_{local} - p_\infty}{q_\infty}$

c local chord, ft

$\bar{c}$ mean aerodynamic chord, ft

d diameter, in.

F_{ej} ejector jet thrust, lb

F_i ideal jet thrust for complete isentropic expansion of the measured primary flow, $w\sqrt{\frac{2R}{g}\frac{\gamma}{\gamma - 1}T_{t,j}\left[1 - \left(\frac{p_\infty}{p_{t,j}}\right)^{\frac{\gamma-1}{\gamma}}\right]}$, lb

g	gravitational acceleration, ft/sec^2
H_2O_2	hydrogen peroxide (90 percent concentration by weight)
i_t	incidence angle of horizontal tail, relative to fuselage center line, deg
l	longitudinal distance from primary jet exit, positive rearward, in.
M	Mach number
m	mass flow, lb-sec/ft
p	static pressure, lb/sq ft
p_t	total pressure, lb/sq ft
$p_{t,j}/p_\infty$	ratio of primary jet total pressure to free-stream static pressure
q	dynamic pressure, lb/sq ft
S	wing area, sq ft
T	temperature, $^{\circ}R$
V	velocity, ft/sec
w	weight flow, lb/sec
w_i	ideal weight flow for choked exit, $p_{t,j}A_p\left(\frac{2}{\gamma + 1}\right)^{\frac{\gamma+1}{2(\gamma-1)}}\sqrt{\frac{\gamma g}{RT_j}}$
$\frac{w_s}{w_p}\sqrt{\frac{T_s}{T_p}}$	corrected secondary-to-primary weight flow ratio
x	longitudinal distance from ejector exit, positive rearward, in.
γ	ratio of specific heats
Λ	sweepback angle

ϕ meridian angle, positive clockwise looking forward from fuselage top center line, deg

Subscripts:

b base

e ejector exit

ej ejector

f primary nozzle flap

i ideal or internal

j jet

m model

p primary

r root

s secondary

t tip or throat

w divergent ejector wall

∞ free stream

APPARATUS AND METHODS

Wind Tunnel and Support System

This investigation was conducted in the Langley 16-foot transonic tunnel, which is a single-return atmospheric wind tunnel with an octagonal slotted test section. It has a speed range from a Mach number of 0.20 to about 1.10, and the Mach number is varied over this range simply by variation of tunnel drive power. The model was supported at the wing tips by a bifurcate sting-support system described in reference 6.

Model

A single-engine fighter-airplane model described in reference 6 was used as a test vehicle for the divergent ejector. Figure 1(a) shows the model mounted in the tunnel test section, and figure 1(b) is a closeup photograph of the divergent ejector installed in the model. Figure 2 is a sketch showing the dimensions and geometric characteristics of the model and the support system. The airplane model was constructed of stainless steel and aluminum, and the wings were rigidly attached to the bifurcate sting support. The fuselage-tail assembly was mounted on a six-component balance which was supported by the wing structure. Two secondary air inlet sizes were used to compare the effect of secondary air quantity on the divergent ejector characteristics. The throat diameters of the two measuring venturis were 0.500 inch and 1.127 inches. Figure 2 shows the inlet with the venturi downstream in the duct leading to the ejector.

Figure 3 is a sketch of the hydrogen peroxide turbojet-engine simulator with the divergent ejector and shows the dimensions as well as the pressure and temperature measurement locations of the divergent ejector. The values of spacing ratio l_e/d_p, diameter ratio d_e/d_p, throat diameter ratio d_t/d_p, and throat spacing ratio l_t/d_p with the primary nozzle closed to the nonafterburner position are also shown in figure 3(b). The ejector was designed for full afterburning operation at a Mach number of 2.0 and $p_{t,j}/p_\infty = 10$, at which the spacing ratio would be 1.0, the diameter ratio, 1.4, throat diameter ratio, 1.16, and the throat spacing ratio, 0.3. The corrected secondary weight flow ratio would be about 6 percent at $M = 2.0$. These ratios correspond closely to those of an ejector designed for $M = 2.0$ shown in reference 2.

Turbojet Simulator

The hydrogen peroxide turbojet-engine simulator described in reference 7 was used for this investigation. The stainless-steel primary convergent nozzle was set at the nonafterburning cruise position (see fig. 3(a)), and the whole simulator system with the divergent ejector was mounted in the model in such a way that the thrust and drag forces on the model and simulator were measured separately (see figs. 2 and 4). Reference 7 shows that this hydrogen peroxide turbojet-engine simulator produces a hot jet exhaust (1,820 °R) which is very similar to the exhaust of a turbojet engine.

Tests

The model was held at zero angle of attack throughout the Mach number range of 0.80 to 1.07. The average Reynolds number based on $\bar{c}$ was 5×10^6. The hydrogen peroxide turbojet-engine simulator was operated at ratios of primary jet total pressure to free-stream static pressure from 1 (jet off) to 5 at all Mach numbers and up to about 9 at Mach numbers above 1.00.

Instrumentation

Pressures were measured on the base of the afterbody, along the inside of the divergent ejector walls, and on the outside of the primary nozzle flap. (See fig. 3(b).) The pressure tubing from these orifices was conducted to the pressure manifold described in reference 8. In addition to the base and ejector pressures, primary jet total and static pressures, secondary air inlet and exit total and static pressures, and primary and secondary total temperatures were measured. (See fig. 3(a).)

A one-component thrust balance measured the thrust forces exerted by the simulator—divergent-ejector system. The six-component-balance forces were also measured but are not reported in this paper.

Data Reduction

Signals produced by electrical pressure transducers in the pressure manifold were transmitted to carrier amplifiers and then to recording oscillographs located in the tunnel control room. The pressures, forces, and temperatures were converted to standard pressure and force coefficients by machine computation from the trace deflections on the paper film.

The thrust force measured on the thrust balance was corrected for the pressure and momentum terms acting on the system to obtain ejector jet thrust in the following manner:

$$F_{ej} = F_{bal} + m_s V_s + (p_s - p_\infty) A_s + (p_i - p_\infty)\left[\frac{1}{2}\left(A_2 + A_1\right)\right] - (p_b - p_\infty)\left[\frac{1}{2}\left(A_2 + A_1\right) - A_e\right]$$

The locations of these pressures and areas are shown in figure 4. It should be noted that the incoming momentum and pressure force of the secondary air system had to be added into the balance measurement to

obtain gross ejector jet thrust. Inspection of the thrust equation shows a pressure force across the flexible diaphragm seal (fig. 4). This pressure force was only a small fraction of the measured thrust, and the exact disposition between the thrust and drag systems was unknown; however, one-half of the small pressure force across the flexible seal was arbitrarily charged to each system. The drag equation presented in reference 8 also contains this pressure term and the term vanishes when drag is subtracted from thrust.

The secondary air was supplied to the ejector from an inlet in the nose of the model, and, consequently, the secondary weight flow varied with Mach number. The secondary weight flow was computed for each test point by using the tunnel stagnation temperature and the total and static pressures measured at the nose venturi. Figure 5 shows the variation of the corrected secondary-to-primary weight flow ratio with jet pressure ratio for all Mach numbers for both the small and the large openings.

Accuracy

The estimated accuracy of the data presented in this paper is as follows:

M	±0.005
C_p	±0.01
F_j, lb	±4
$p_{t,j}/p_\infty$	±0.1
$\frac{w_s}{w_p}\sqrt{\frac{T_s}{T_p}}$	±0.01

RESULTS AND DISCUSSION

Primary Nozzle Discharge Coefficient

The measured weight flow through the primary nozzle is compared with the ideal weight flow through the nozzle based on measured pressure and temperature in figure 6. The data are an average for all jet total pressure ratios at each Mach number, and the discharge coefficient decreases from about 0.94 at $M = 0.80$ to 0.92 at $M = 1.07$. These data are in only fair agreement with the expected coefficients from convergent nozzles and may be low because the convergence angle of the nozzle is large (37°). (See ref. 9.)

Ejector and Base Pressure Coefficients

Base pressure coefficients.- Figures 7 and 8 show the variation of average base pressure (average for 5 meridians) with Mach number and the variation of the base pressure coefficient at $\phi = 352^{\circ}$ with the ejector wall pressure coefficient measured at $x = -0.13$. Figure 7 indicates that the average base pressure coefficient is established largely by the external flow. (Note scale zero shift for each pressure ratio.) The jet-off value of $C_{p,b}$ becomes positive near sonic speed as the configuration shock moves to the base regions and then becomes negative at low supersonic speeds when the shock emanates from the trailing mixing region. The level of the base pressure coefficients is altered from the jet-off position by jet operation, as is shown in figure 7 for the lines of constant jet pressure ratio. It is noted that the addition of larger quantities of secondary flow (large opening) has a beneficial effect on base pressure coefficient in most instances.

In figure 8 the base pressure coefficient at $\phi = 352^{\circ}$ follows the internal ejector pressure coefficient rather closely. As the primary jet pressure ratio increases and the primary jet starts to pump on the secondary system, the ejector pressure is reduced and so is the base pressure. This is a typical result found in isolated body jet exit investigations when the ratio of the base or model to jet size is large (on the order of 3 or 4). In general, operation of the jet at these off-design conditions had a detrimental effect on the base pressure coefficient and would have increased the base pressure drag of the configuration. At the design condition, the full afterburning jet would completely fill the ejector nozzle and the ejector exit and base pressure would be nearly equal to p_{∞}. Any increase in jet total pressure ratio above the design value could then produce positive exit and base pressures. (See ref. 10.)

Ejector pressure coefficients.- Figure 9 shows the pressure coefficients measured along the divergent ejector wall and across the primary nozzle flap plotted against distance from the ejector exit for nominal values of jet pressure ratio and constant Mach numbers. The addition of large quantities of secondary air as shown by the tailed symbols tended to increase the level of the pressures except near a Mach number of 1.0 where the pressures were already positive with the small opening. This pressure increase was probably caused by the large quantity of secondary flow acting like a base bleed and reducing the pumping action of the primary jet on the secondary flow.

When the Mach number was increased above 1.0 and the jet pressure ratio was increased to about 8.5, the wall pressures became very negative in the vicinity of the primary exit. The wall pressure coefficients then showed a tendency to increase until near $x = -1.0$, where they decreased sharply again.

Some jet boundaries were estimated by using the method of reference 11 and the shape parameters for H_2O_2 presented in figure 2 of reference 7. It was assumed that the jet was exhausting into still air, and these calculated jet boundaries are shown in figure 10 for ratios of jet total pressure to free-stream static pressure of 5, 9, and 12. It can be seen that the boundary for jet pressure ratios of 5 and 9 does not approach the wall of the divergent ejector. Since the wall pressure distribution seems to indicate jet attachment near a pressure ratio of 8.5, as evidenced by a sharp increase (see fig. 9 for $M = 1.04$) as the secondary air is squeezed into a smaller and smaller area and then an expansion after jet attachment, it is reasoned that the effective jet pressure ratio must be greater than 9. It is noted that the ratio of the jet total pressure to the average pressure over the primary nozzle flap and at the ejector throat is about 12. With this value as the actual jet pressure ratio, the calculated jet boundary for 12 intersects the ejector wall near $x = -1.0$. Inspection of the pressure-coefficient data, as stated previously, indicates an expansion from this point toward the exit, and the jet is probably attached to the wall and is seriously overexpanded. At $p_{t,j}/p_\infty = 8.5$, the addition of larger quantities of secondary air, particularly at $M = 1.00$, caused the wall pressures to become much more positive, very probably because the primary jet was forced away from the ejector walls and did not attach at this pressure ratio.

Ejector Jet Thrust Characteristics

The variation of ejector jet thrust with jet pressure ratio is shown in figure 11 for all test Mach numbers. The ideal jet thrust that would have resulted from isentropic expansion of the measured primary weight flow is also shown for comparison. It should be noted that this comparison is valid for zero secondary air flow and is probably good for low values of secondary weight flow; however, when large quantities of secondary air are introduced, this comparison is fictitious since no account is made of the ideal thrust available from expansion of the secondary flow.

These data indicate that the addition of large quantities of secondary air raised the jet thrust by raising the static pressures along the ejector walls. The data also indicate that the ejector jet thrust approaches the ideal primary thrust more closely when the external flow raised the level of the base and ejector pressure coefficients. When the Mach number was increased to 1.07, the thrust decreased considerably below the ideal values, because the external flow reduced the pressures in the separated regions along the divergent ejector walls, except at

the highest pressure ratio where the jet was probably attached but was seriously overexpanded.

Jet Thrust Ratio

The variation of jet thrust ratio with Mach number for constant values of jet pressure ratio is shown in figure 12. (Note scale zero shift for each pressure ratio.) These data indicate that Mach number and quantity of secondary air have a large effect on jet thrust ratio. These values of jet thrust ratio for constant values of jet pressure ratio are not significant outside the operating limits for the turbojet engine; therefore, the jet thrust ratio is presented in figure 13 for a typical schedule of turbojet-engine pressure ratio with Mach number. If the cruise speed is selected as $M = 0.90$, the jet thrust ratio is 0.92 with a secondary weight flow ratio of 0.033 (fig. 5(a)). This ratio is increased to 0.96 by an increase of about 0.14 in corrected secondary weight flow ratio (20 percent increase in w_s); however, it should be remembered that the net thrust ratio will decrease with these larger quantities of secondary flow.

The jet thrust ratio for a conical ejector (ref. 3) operating at these same conditions (0.03 secondary weight flow ratio) is also shown in figure 13 for comparison. With a corrected secondary-to-primary weight flow ratio of 0.033, the divergent ejector jet thrust is 5 percent lower than the conical ejector at a Mach number of 0.90. Reference 2 indicates that the net thrust ratio for a fixed divergent ejector at these off-design conditions is very low in comparison with that for a conical or cylindrical ejector. The net thrust ratio for the divergent ejector, assuming that all of the secondary air was taken from the free stream at full ram pressure, has been calculated to be 0.86 for the small opening at $M = 0.90$, $p_{t,j}/p_\infty = 3.62$. For the large opening at the same conditions, the net thrust ratio is 0.76. Data taken from reference 2 for a cylindrical ejector indicate a net thrust ratio of 0.96, and this shows that this particular divergent ejector operating with a nonafterburning primary nozzle at $\frac{w_s}{w_p}\sqrt{\frac{T_s}{T_p}} = 0.033$ has 10 percent less net thrust than a cylindrical ejector which is operating very near its design point.

The data of figure 13 also indicate that poor thrust performance might be obtained if the primary nozzle was not opened to the full afterburner position at a Mach number of about 0.98. When the nozzle is opened for full afterburner, the net thrust performance should increase significantly, as indicated in the data of reference 2.

CONCLUDING REMARKS

A brief investigation of a fixed divergent ejector installed in a single-engine fighter model has been conducted in the Langley 16-foot transonic tunnel. The ejector was designed for full afterburning operation at a Mach number of 2.0, but was operated only in the off-design nonafterburning cruise condition for this investigation. The Mach number range was from 0.80 to 1.07 at primary jet total pressure ratios up to about 9.

The results of the investigation indicated that the addition of large quantities of secondary air (14 percent increase in corrected secondary weight flow ratio) would relieve the adverse effects of jet pumping on the divergent ejector walls. It was found that external flow set the base pressure level at each Mach number and that primary jet flow had a detrimental effect on the base pressure at these off-design conditions. The jet thrust performance of the fixed divergent ejector was about 5 percent less than that of a conical ejector at a Mach number of 0.90. It was indicated that the thrust performance of an airplane equipped with this ejector might be poor if full afterburning operation was not started at a Mach number of about 0.98.

Langley Aeronautical Laboratory,
National Advisory Committee for Aeronautics,
Langley Field, Va., Nov. 22, 1957.

REFERENCES

1. Krull, H. George, and Steffen, Fred W.: Performance Characteristics of One Convergent and Three Convergent-Divergent Nozzles. NACA RM E52H12, 1952.

2. Greathouse, William K., and Beale, William T.: Performance Characteristics of Several Divergent-Shroud Aircraft Ejectors. NACA RM E55G21a, 1955.

3. Fleming, William Adam: Internal Performance of Several Types of Jet-Exit Configurations for Supersonic Turbojet Aircraft. NACA RM E52K04, 1953.

4. Hearth, Donald P., and Wilcox, Fred A.: Thrust and Drag Characteristics of a Convergent-Divergent Nozzle With Various Exhaust Jet Temperatures. NACA RM E53L23b, 1954.

5. Ashwood, P. F., Crosse, G. W., and Goddard, Jean E.: Measurements of the Thrust Produced by Convergent-Divergent Nozzles at Pressure Ratios Up to 20. C.P. No. 326, British A.R.C., 1957.

6. Norton, Harry T., Jr., and Swihart, John M.: Effect of a Hot-Jet Exhaust on Pressure Distributions and External Drag of Several Afterbodies on a Single-Engine Airplane Model at Transonic Speeds. NACA RM L57J04, 1957.

7. Runckel, Jack F., and Swihart, John M.: A Hydrogen Peroxide Turbojet-Engine Simulator for Wind-Tunnel Powered-Model Investigations. NACA RM L57H15, 1957.

8. Swihart, John M.: Effect of Target-Type Thrust Reverser on Transonic Aerodynamic Characteristics of a Single-Engine Fighter Model. NACA RM L57J16, 1957.

9. Krull, H. George, and Beale, William T.: Internal Performance Characteristics of Short Convergent-Divergent Exhaust Nozzles Designed by the Method of Characteristics. NACA RM E56D27a, 1956.

10. Boughman, L. Eugene, and Kochendorfer, Fred D.: Jet Effects on Base Pressures of Conical Afterbodies at Mach 1.91 and 3.12. NACA RM E57E06, 1957.

11. Love, Eugene S., and Grigsby, Carl E.: Some Studies of Axisymmetric Free Jets Exhausting From Sonic and Supersonic Nozzles Into Still Air and Into Supersonic Streams. NACA RM L54L31, 1955.

(a) Three-quarter front view. L-92106

Figure 1.- Photograph of model with divergent ejector located in test section of Langley 16-foot transonic wind tunnel.

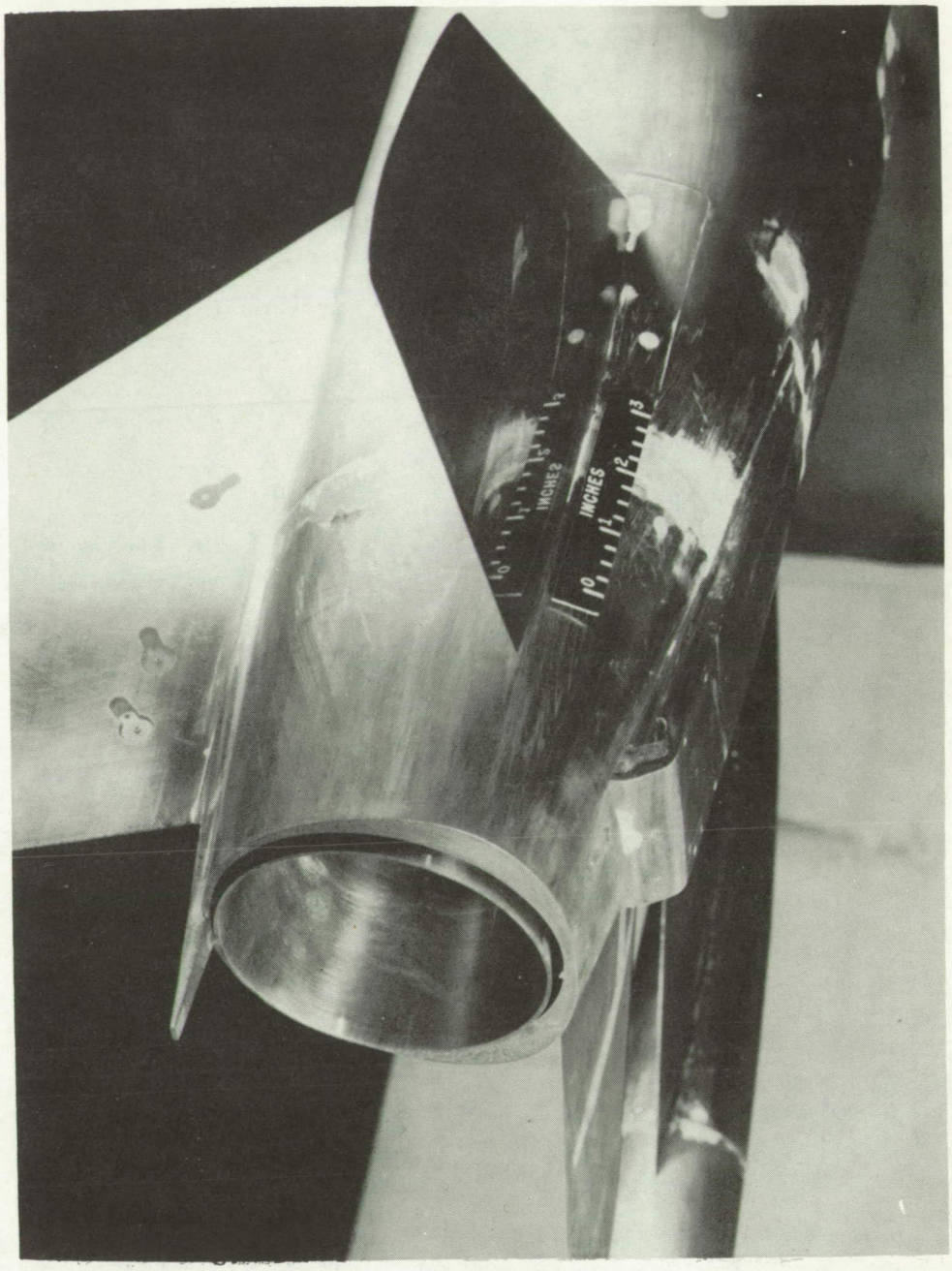

(b) Three-quarter rear view showing ejector exit. L-95253

Figure 1.- Concluded.

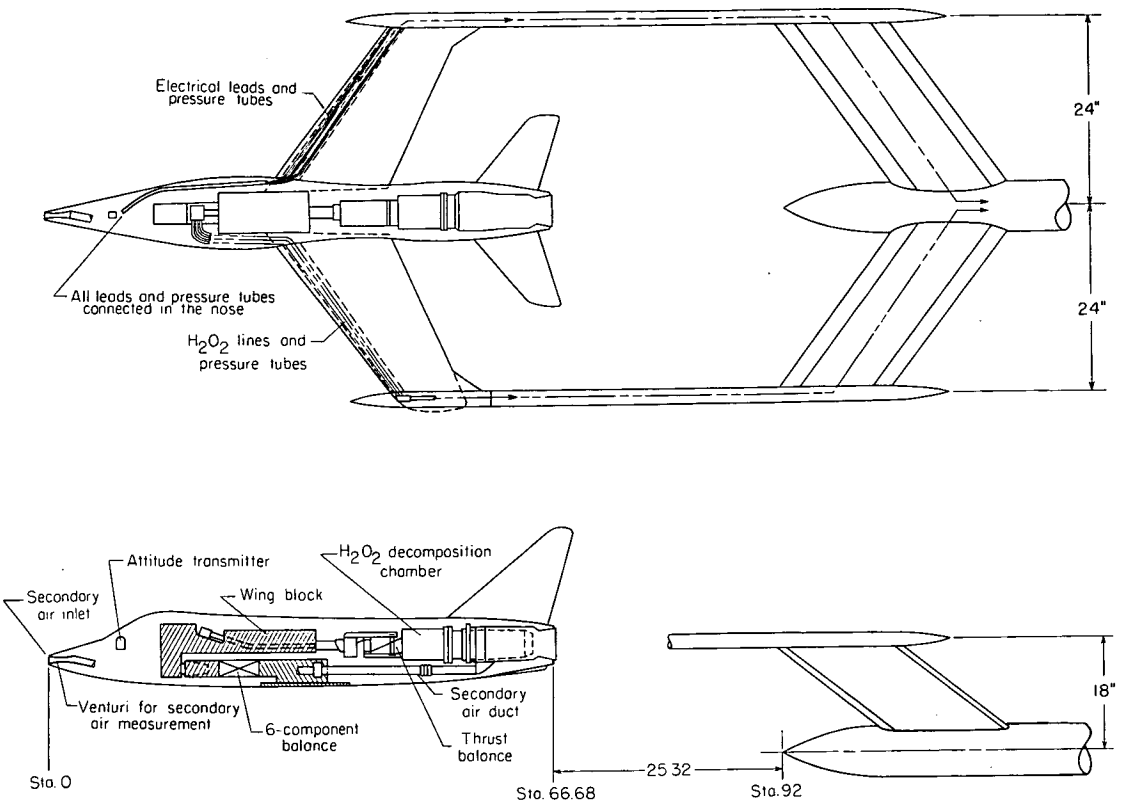

FUSELAGE	
Length	66.68 in.
Max. height	9.0 in.
Max. width	8.6 in.
Area ruled for M = 1.0	

WING	
Wing area, (nominal), S	4.44 sq ft
AR	4.00
$\Lambda_{c/4}$	35°
c_r	17.273 in.
c_t	8.636
NACA 65A006 airfoil sections-streamwise with 2.4% leading edge camber	
Taper ratio	0.50
A_j/S (nonafterburning)	0.0051

VERTICAL TAIL	
$\Lambda_{c/4}$	44°, 27"
Root section	NACA 0006
Tip section	NACA 0006
c_r	14.000 in.
c_t	2.480 in.
Taper ratio	0.18

HORIZONTAL TAIL	
$\Lambda_{c/4}$	35°
Root section	NACA 65A006
Tip section	NACA 65A004
c_r	9.893 in.
c_t	3.960 in.
AR	3.50
Taper ratio	0.40
i_t	-1.50°

Figure 2.- Sketch of jet exhaust simulator model and support system.

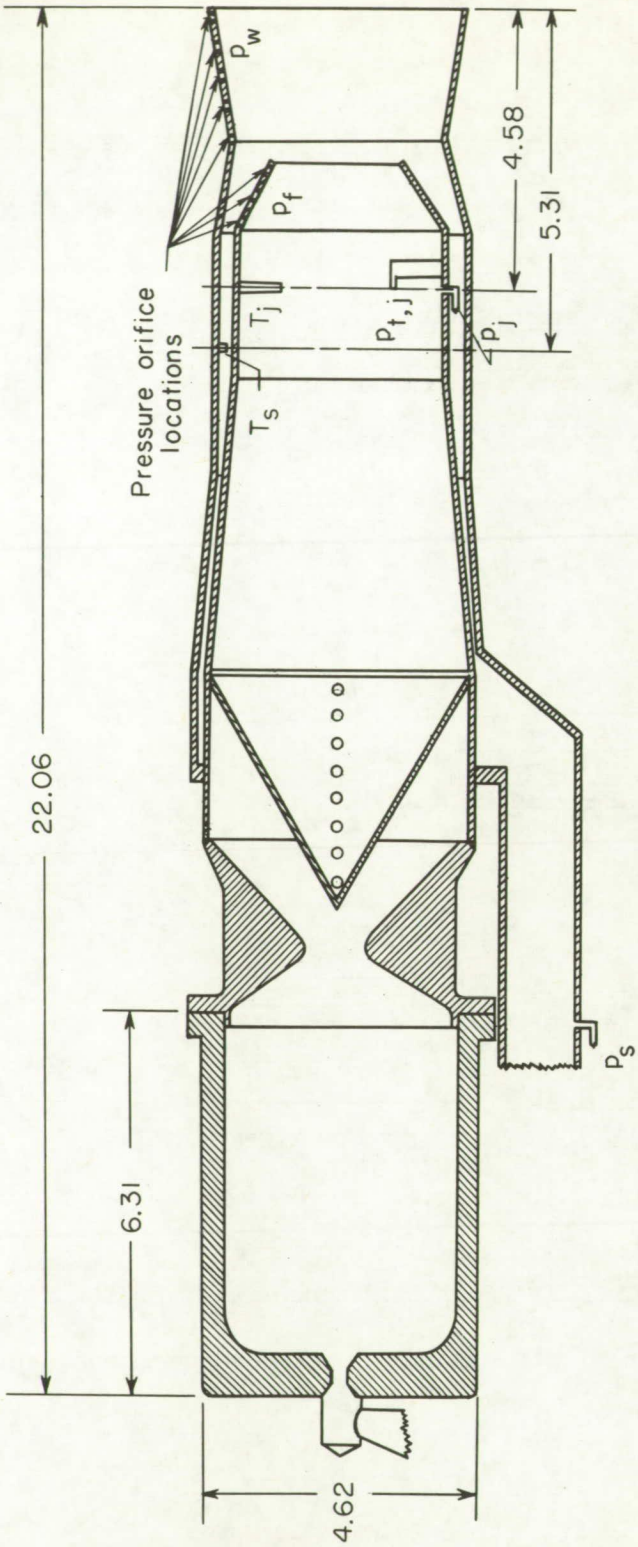

(a) Simulator dimensions and primary and secondary flow instrumentation locations.

Figure 3.- Sketch of hydrogen peroxide turbojet-engine simulator with instrumentation details. All dimensions are in inches.

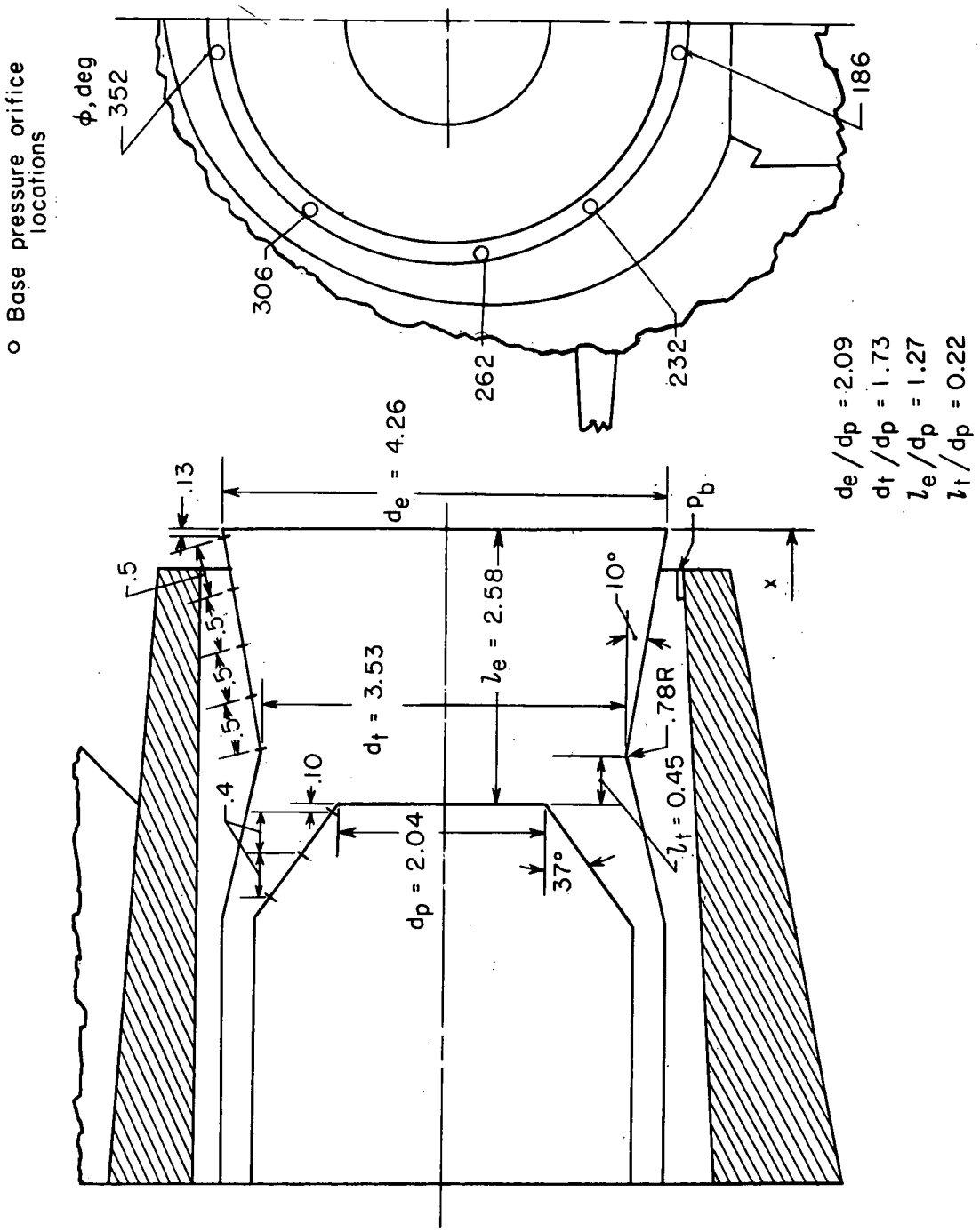

(b) Ejector dimensions and ejector and base pressure orifice locations.

Figure 3.- Concluded.

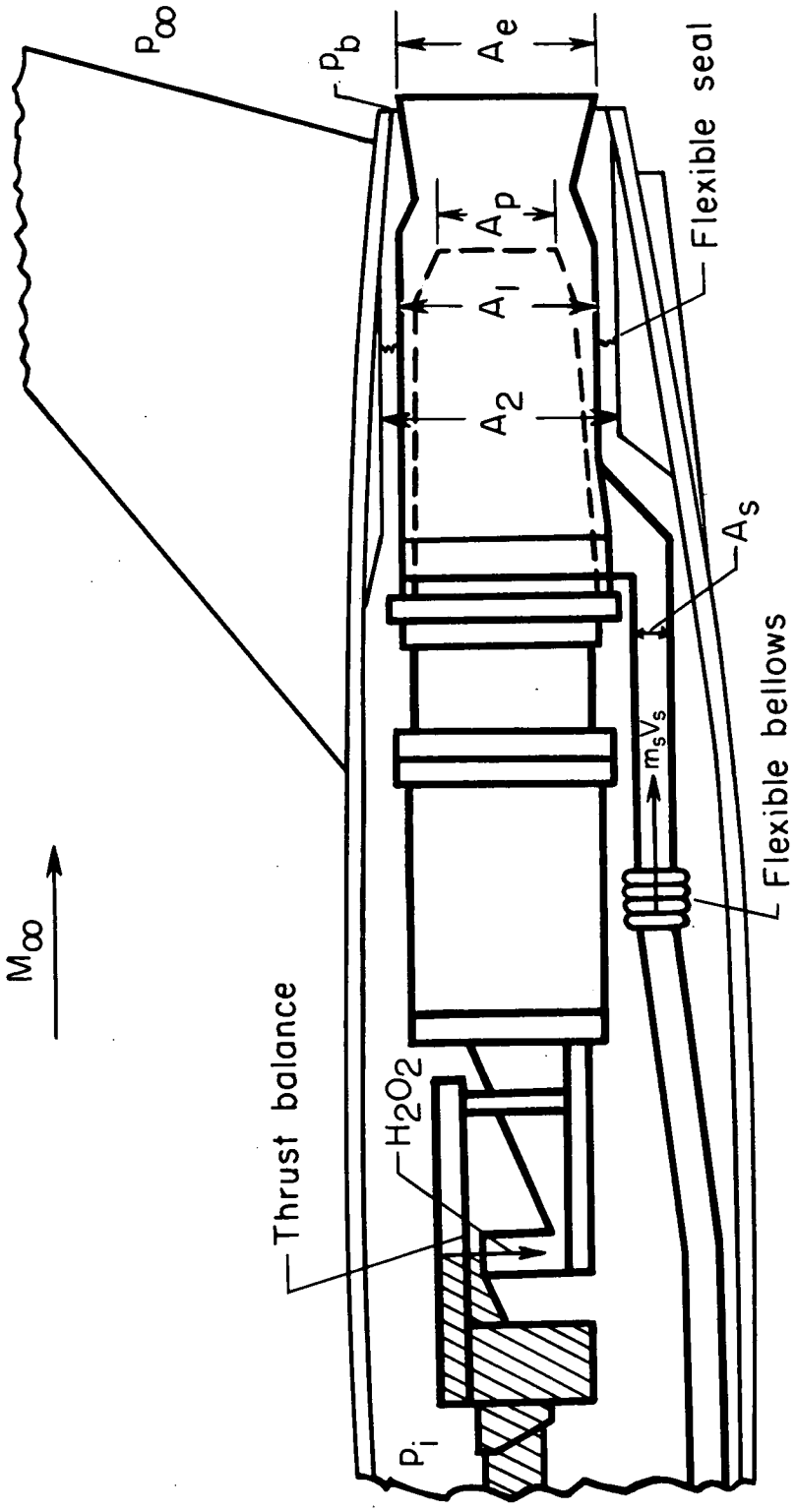

Figure 4.- Schematic diagram of thrust system.

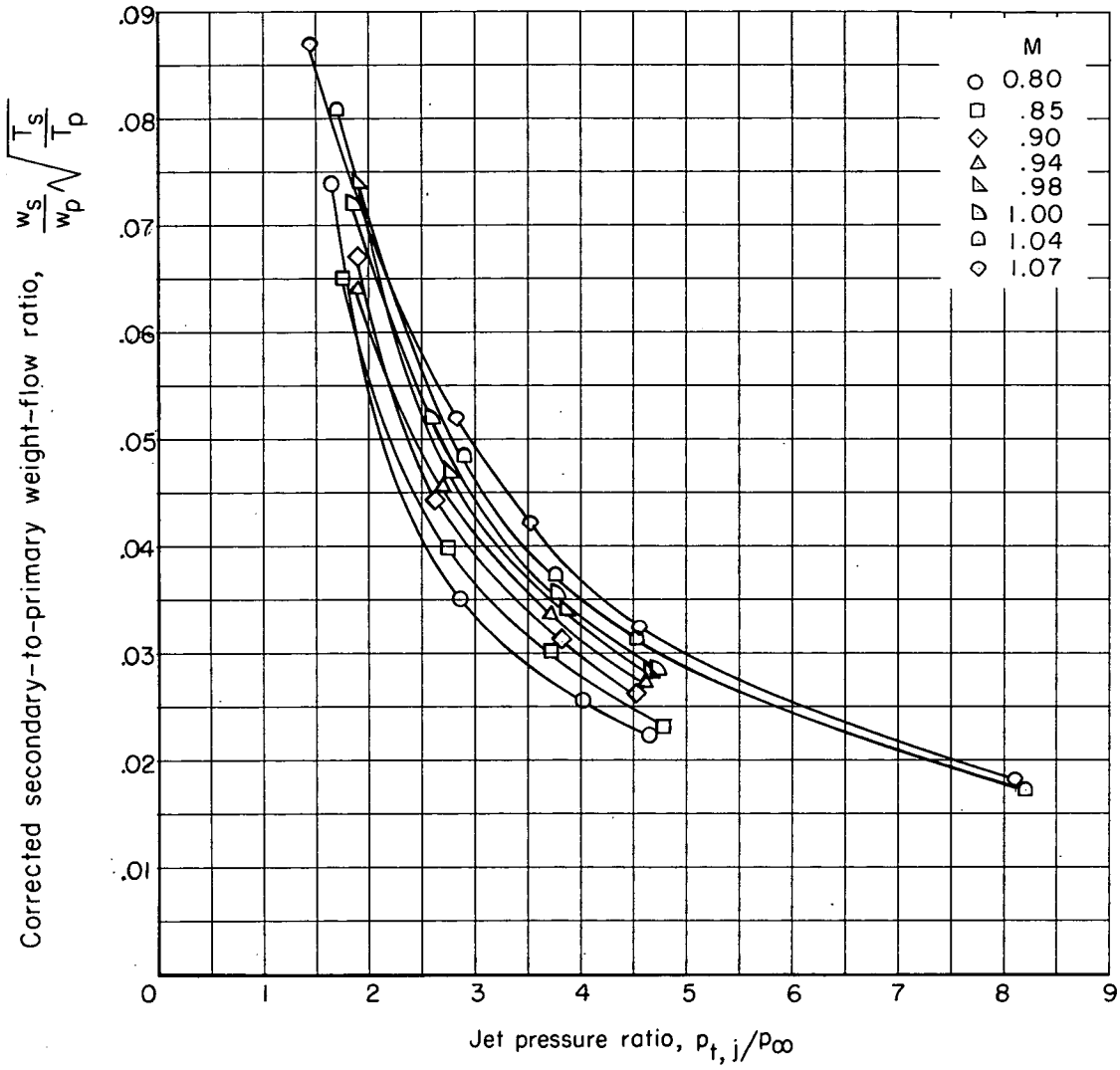

(a) Small opening in secondary air duct (d = 0.500 in.).

Figure 5.- Variation of corrected secondary-weight-flow ratio with jet-pressure ratio for Mach number range.

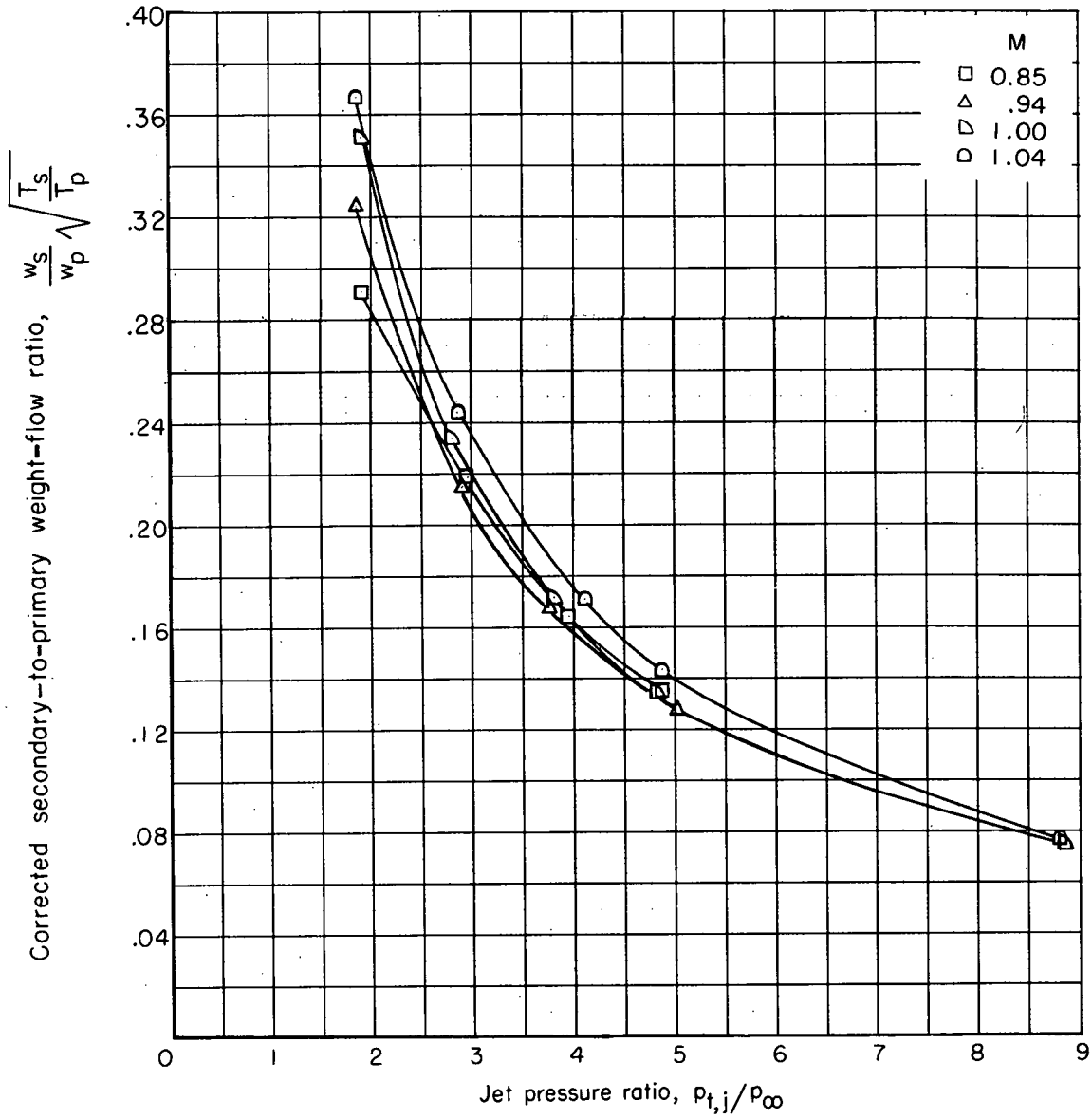

(b) Large opening in secondary air duct (d = 1.127 in.).

Figure 5.- Concluded.

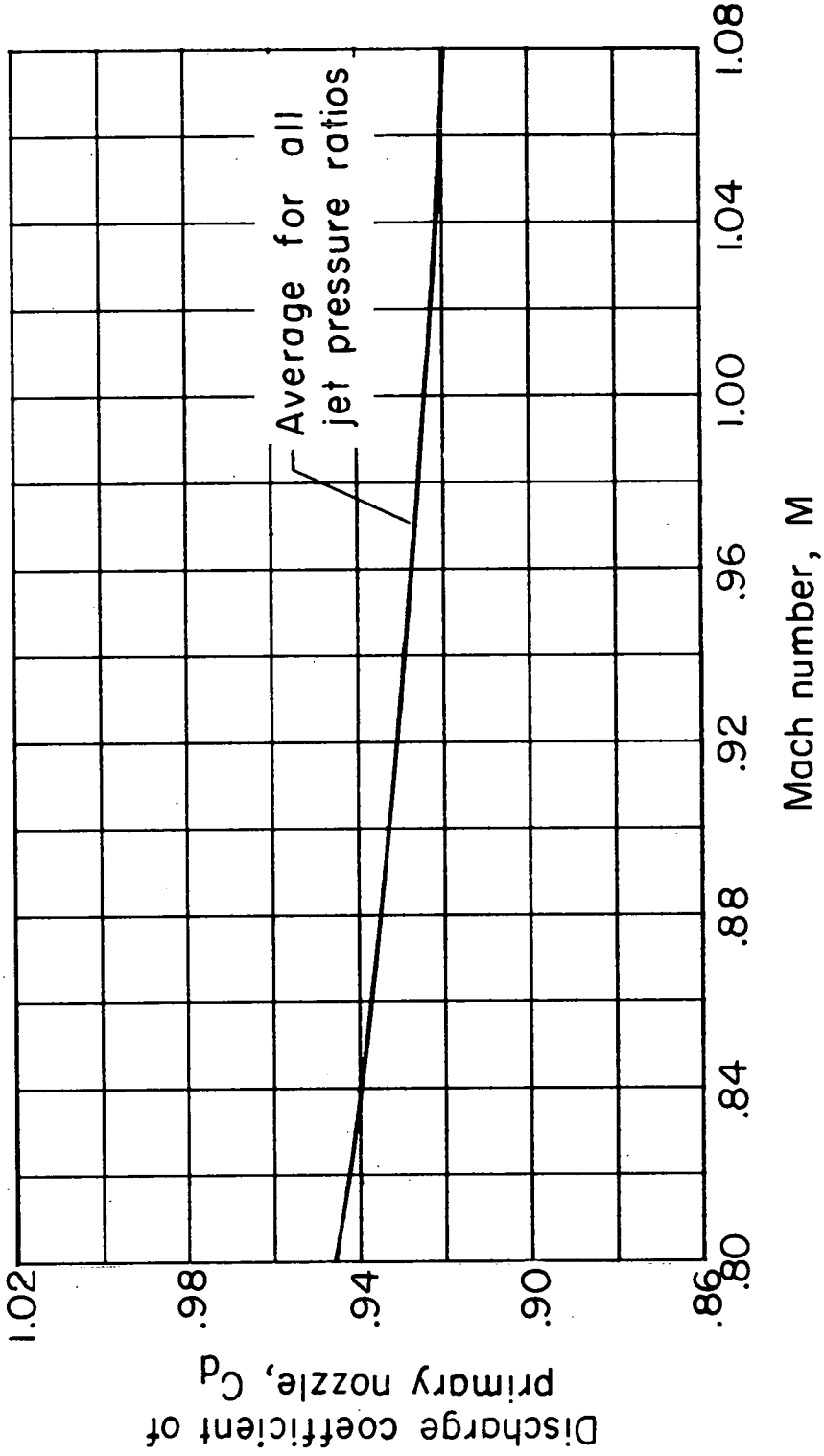

Figure 6.- Variation of primary nozzle discharge coefficient with Mach number.

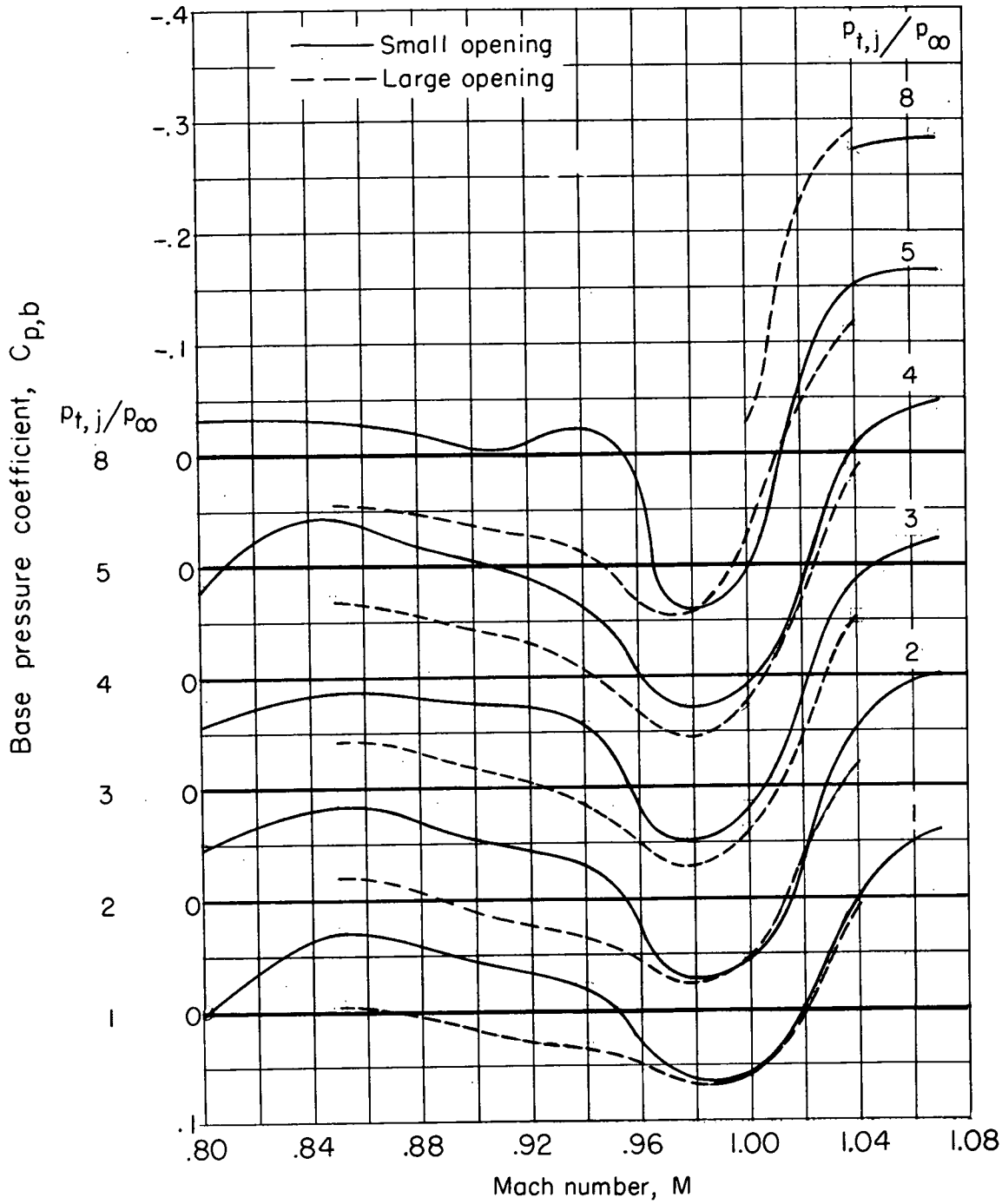

Figure 7.- Effect of Mach number on average base pressure coefficient for several jet pressure ratios.

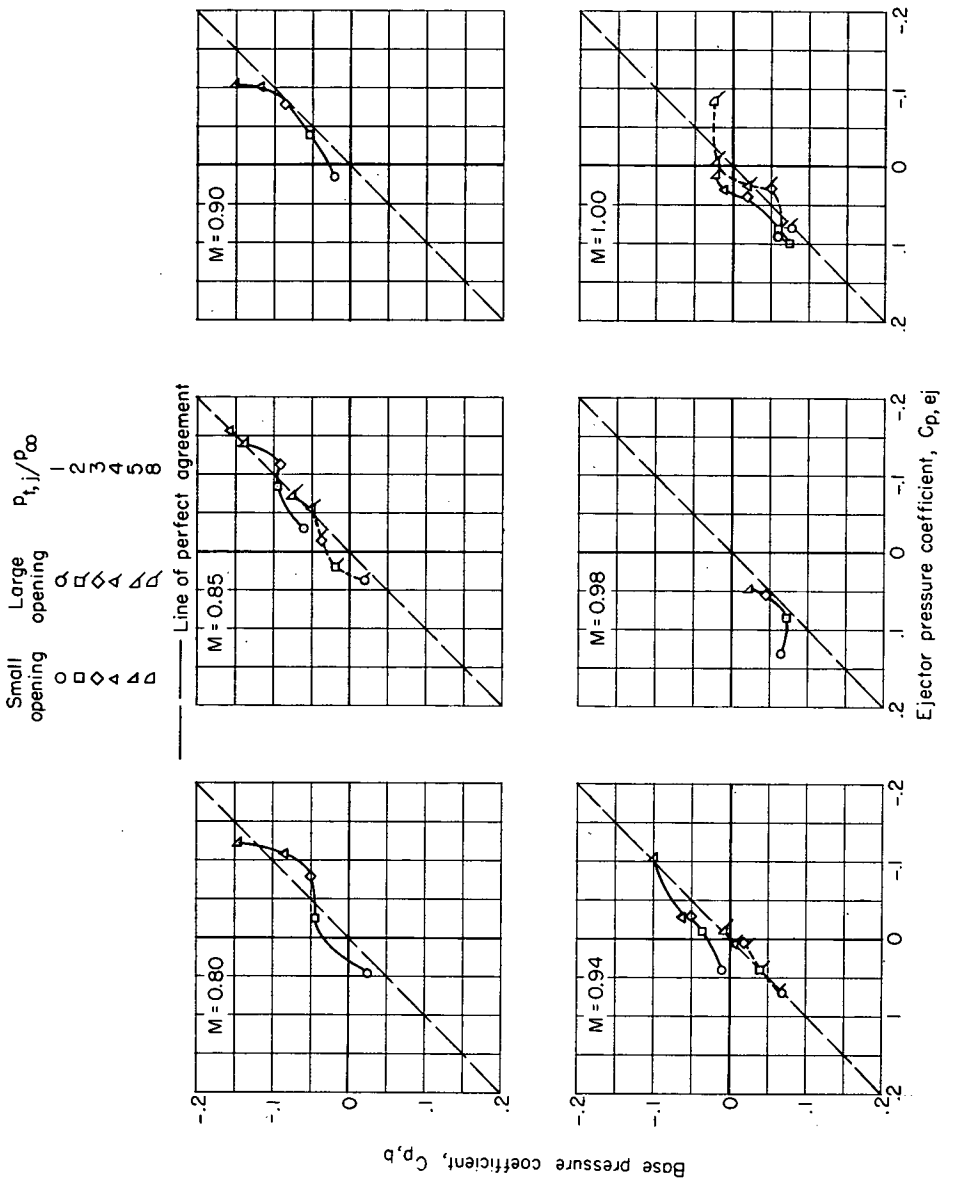

(a) M = 0.80 to 1.00.

Figure 8.- Variation of base pressure coefficient at $\phi = 352^\circ$ with ejector wall pressure coefficient at x = -0.13 inch for transonic Mach number range.

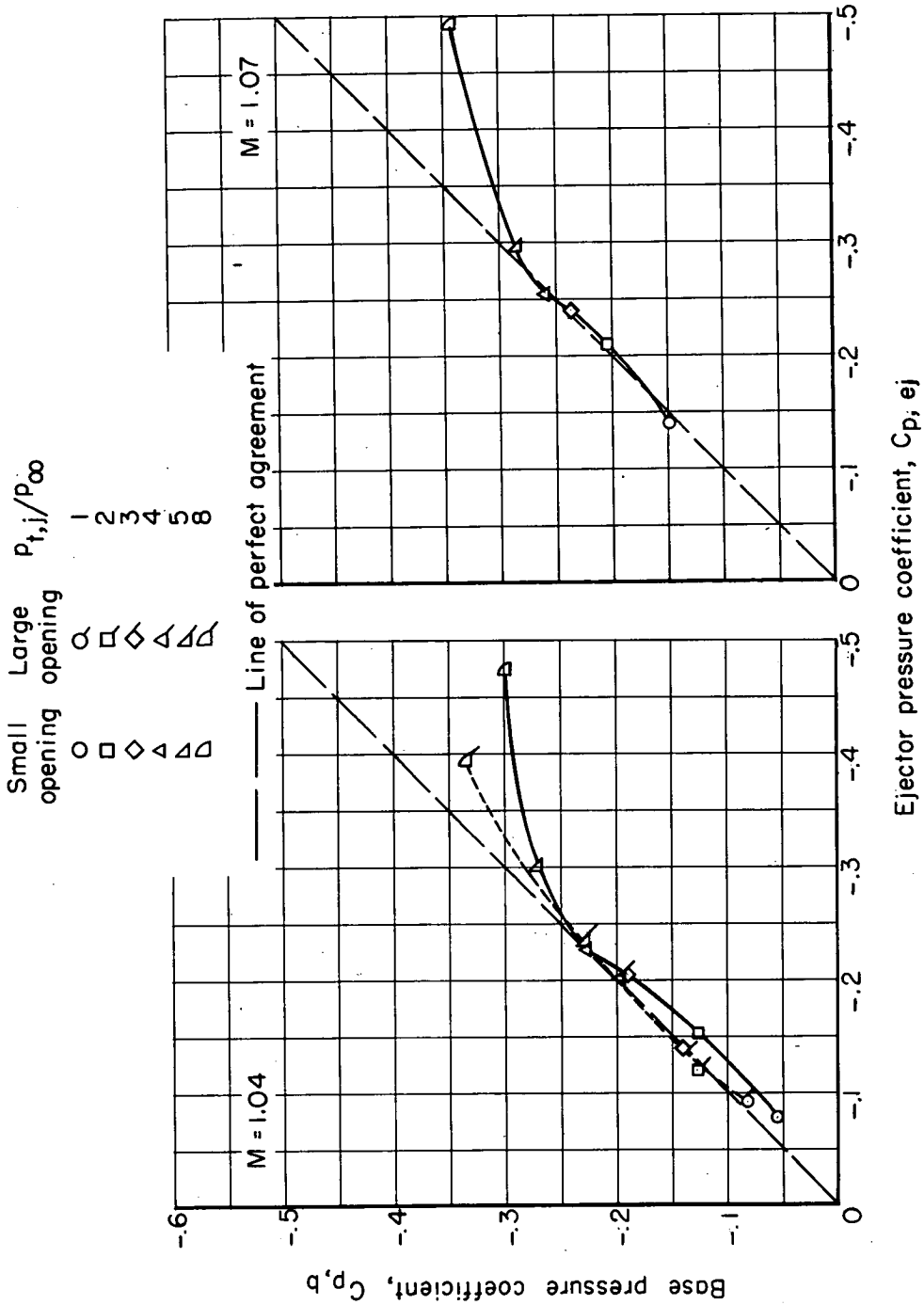

(b) M = 1.04 and 1.07.

Figure 8.- Concluded.

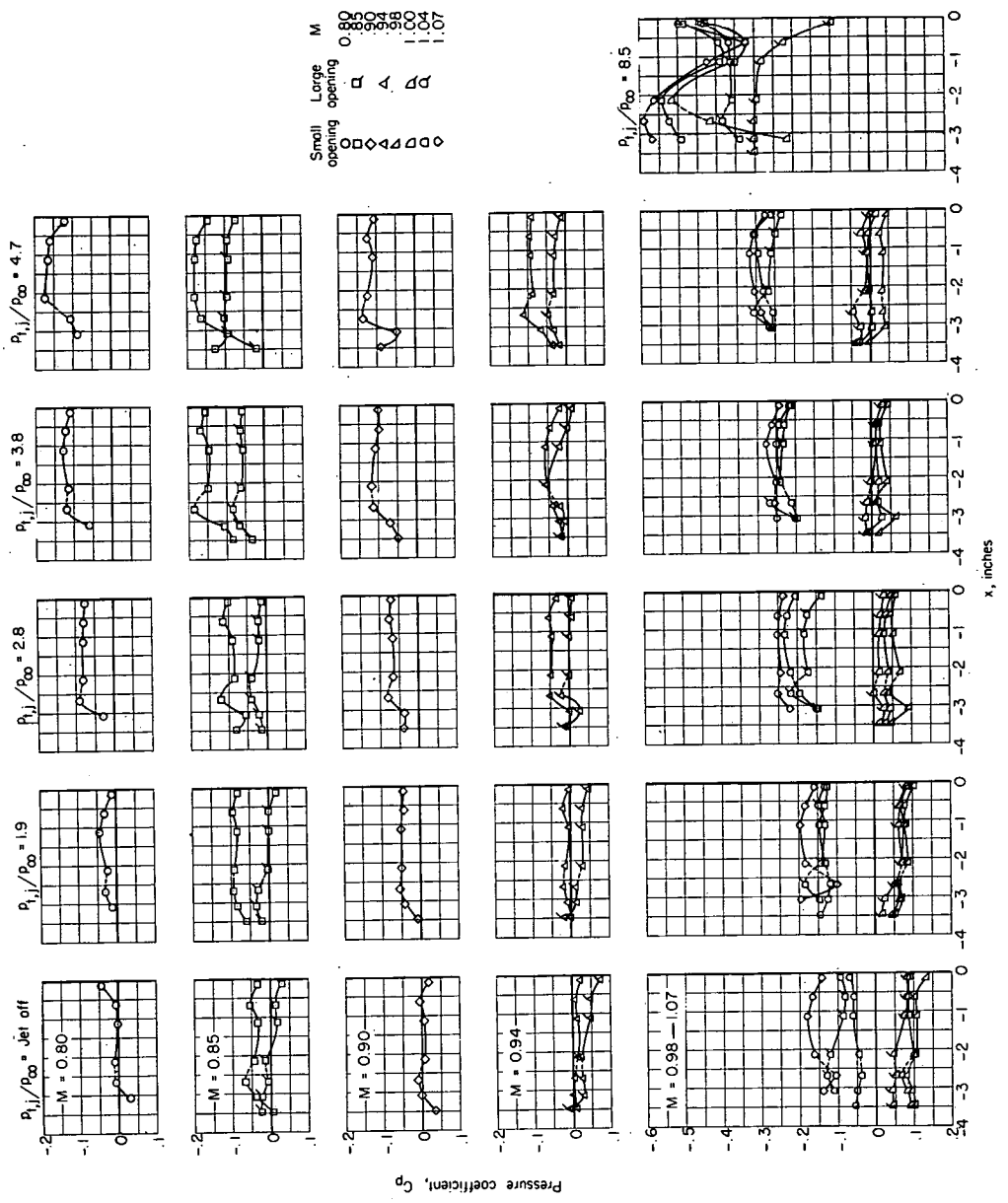

Figure 9.- Effect of jet-total pressure ratio on local pressure coefficients along primary nozzle flap and divergent ejector wall. Values of jet-pressure ratios are nominal.

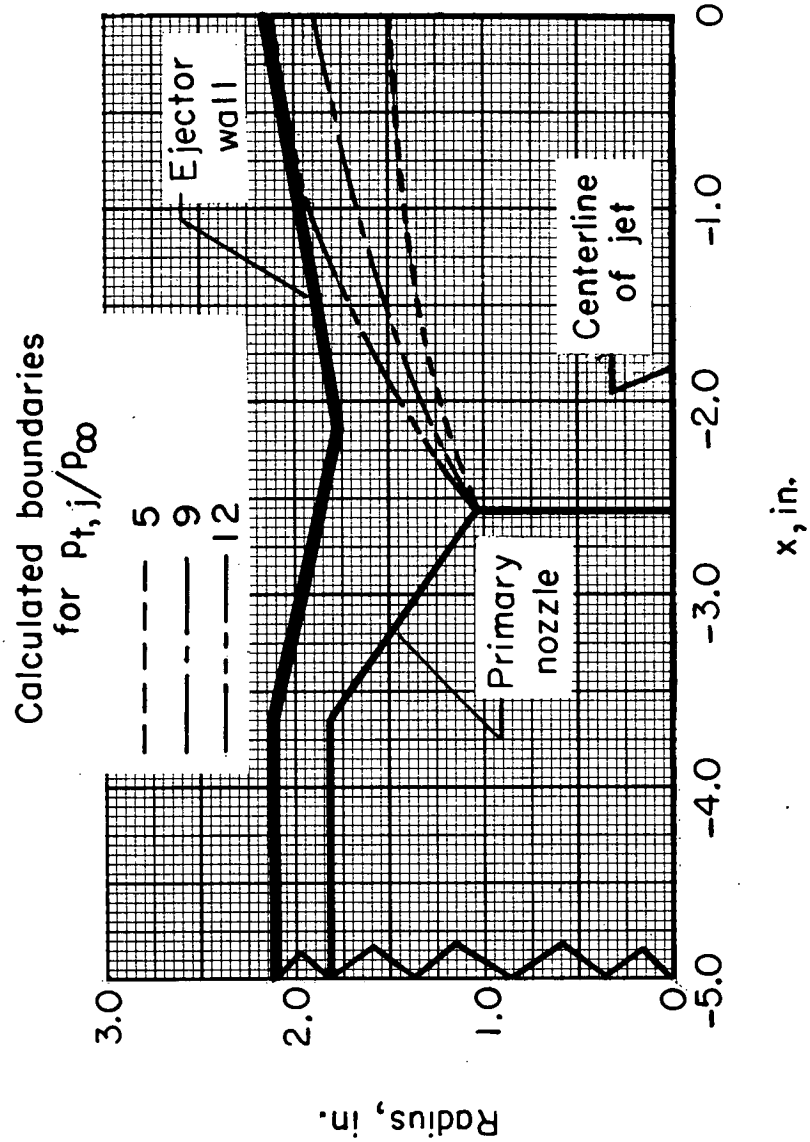

Figure 10.- Sketch of calculated jet boundaries inside divergent ejector. Boundaries calculated by method of reference 11.

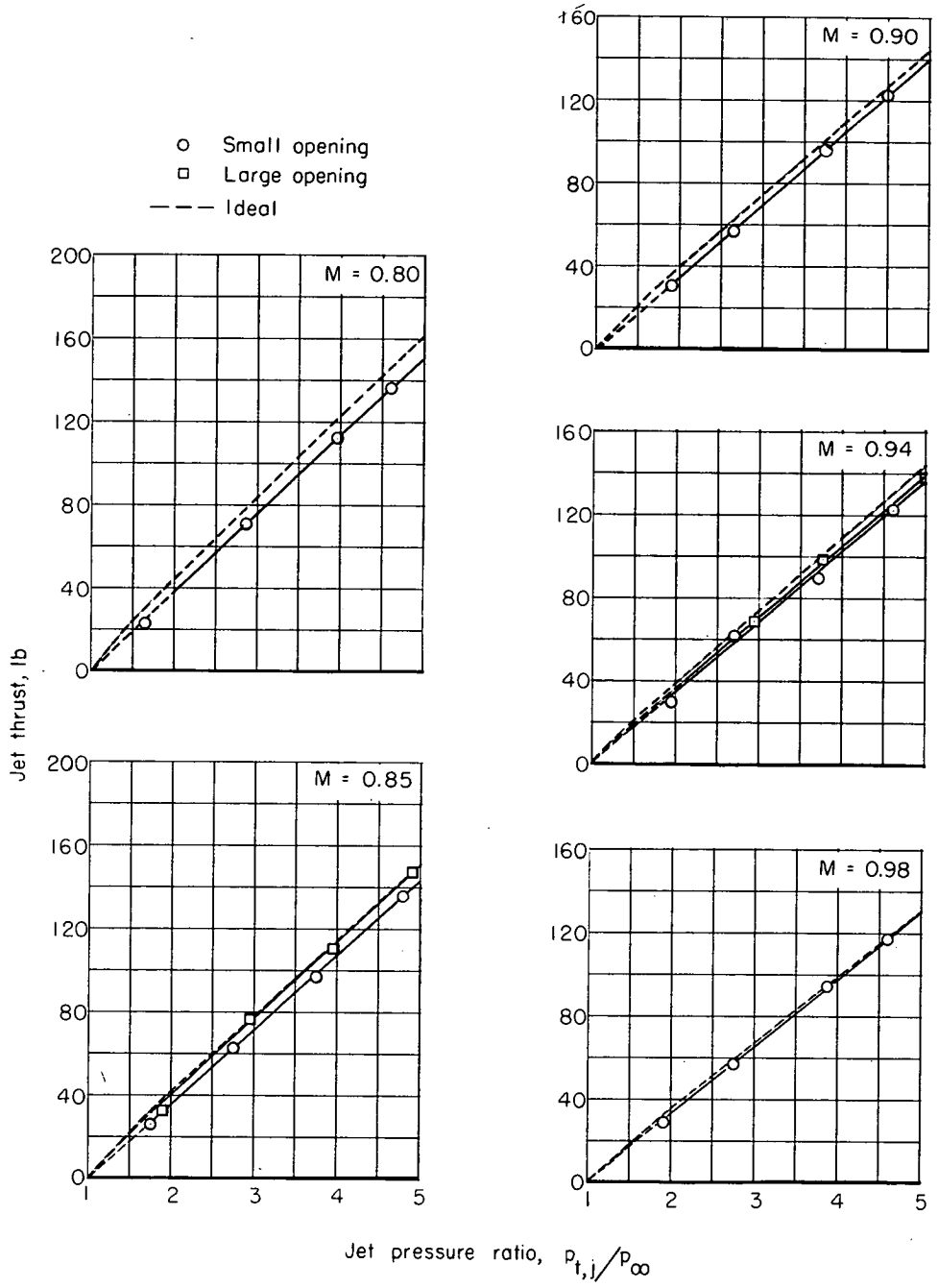

(a) M = 0.80 to 0.98.

Figure 11.- Variation of ejector jet thrust with jet pressure ratio for constant Mach numbers and comparison with ideal primary jet thrust.

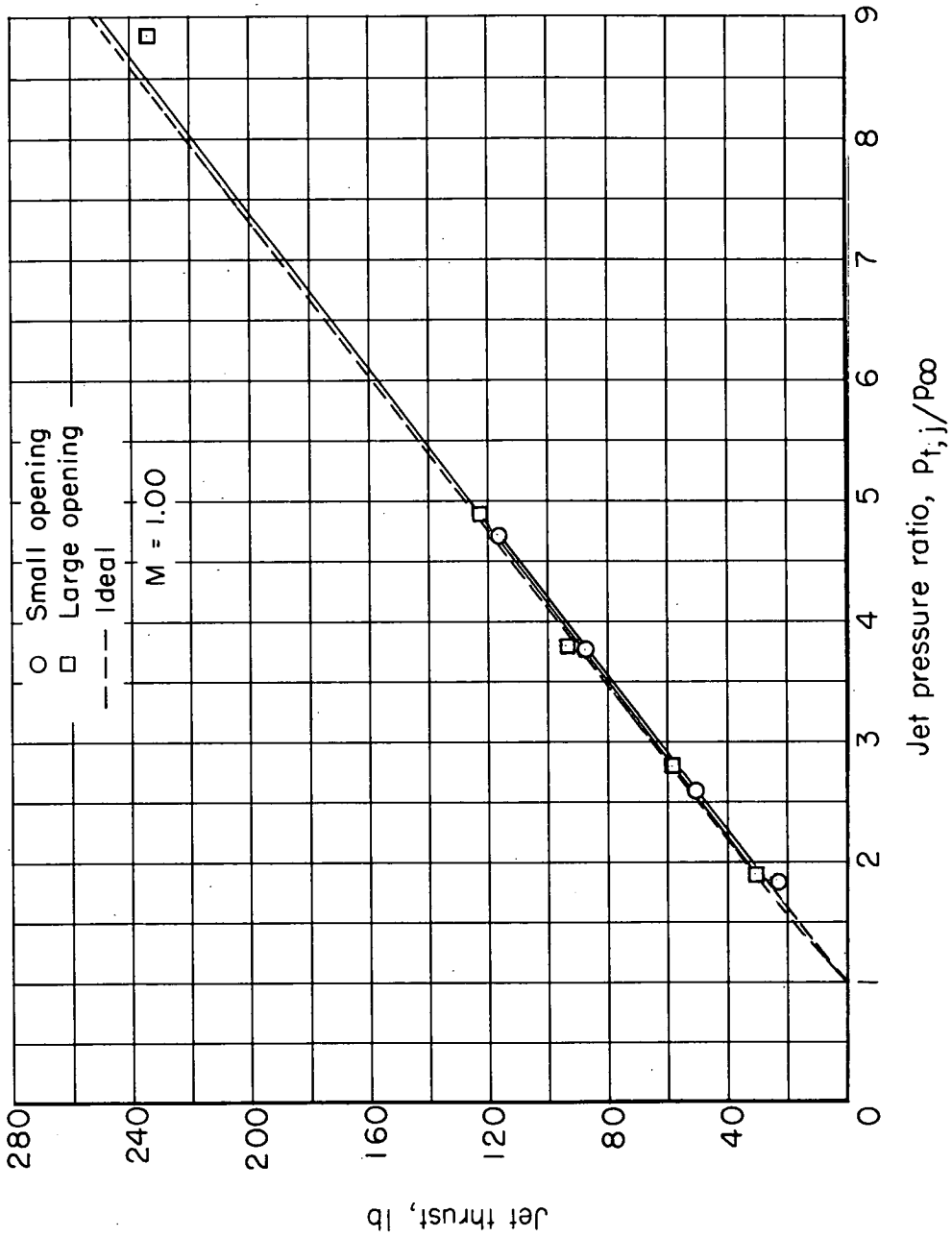

(b) M = 1.00.

Figure 11.- Continued.

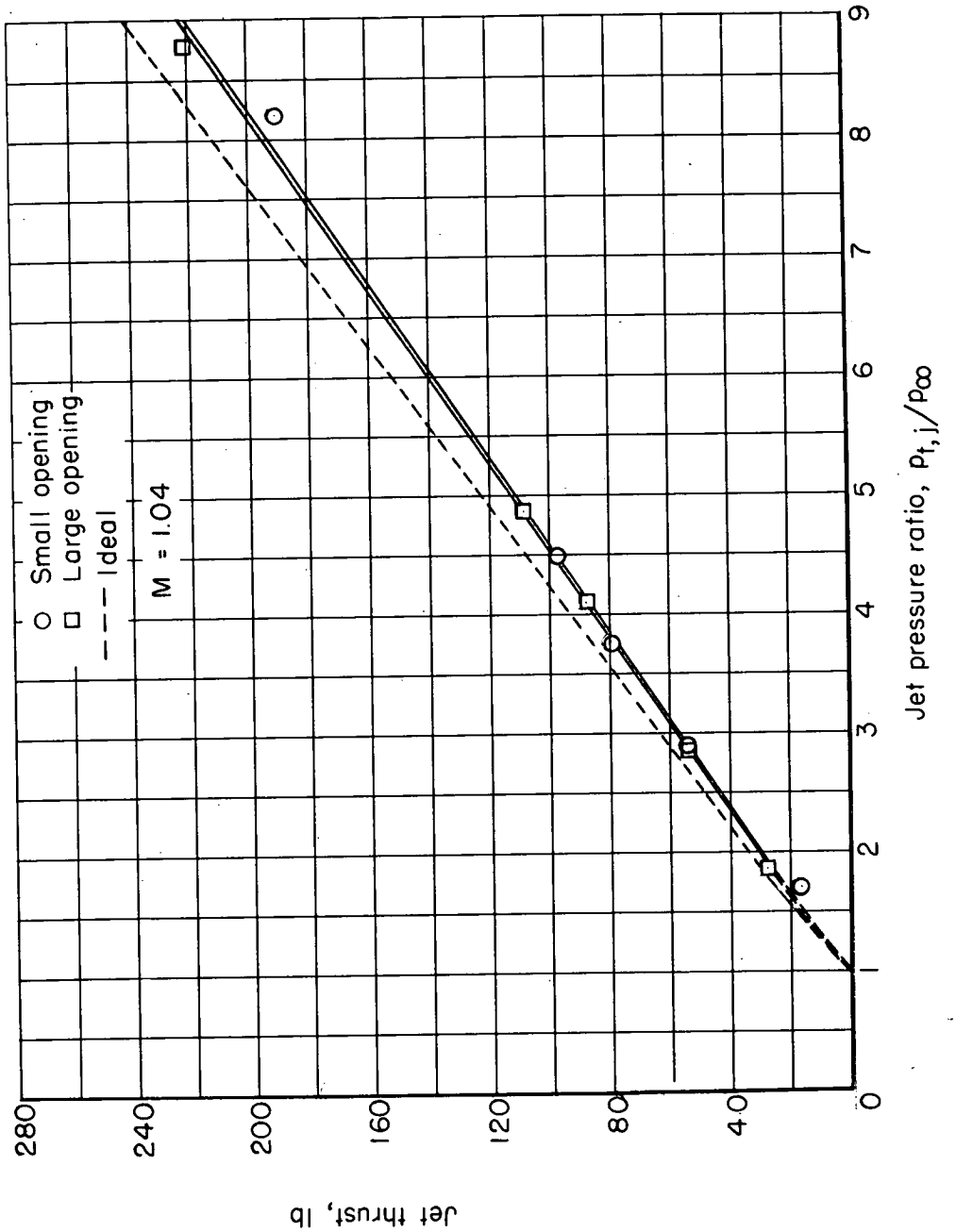

(c) M = 1.04.

Figure 11.- Continued.

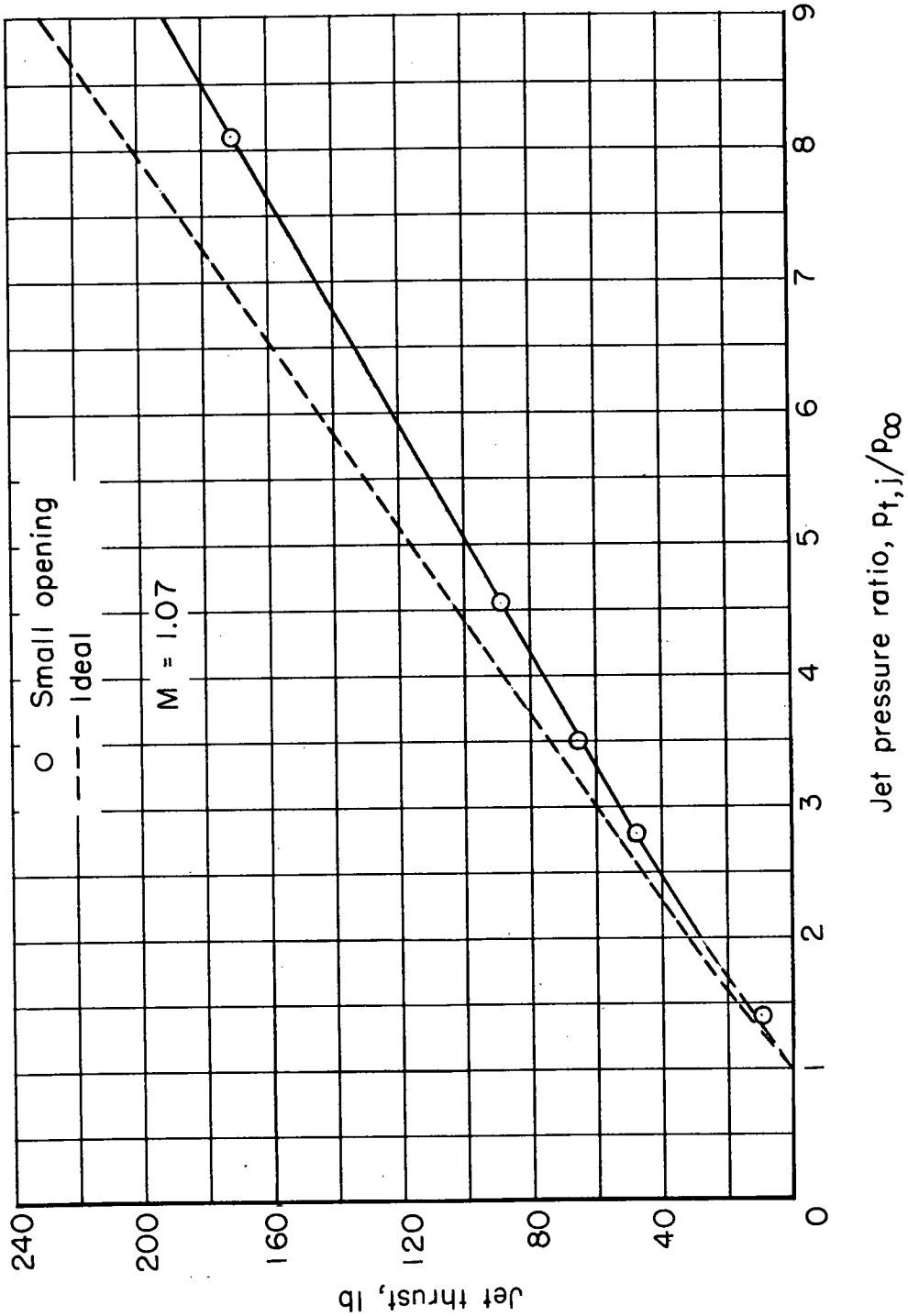

(d) M = 1.07.

Figure 11.- Concluded.

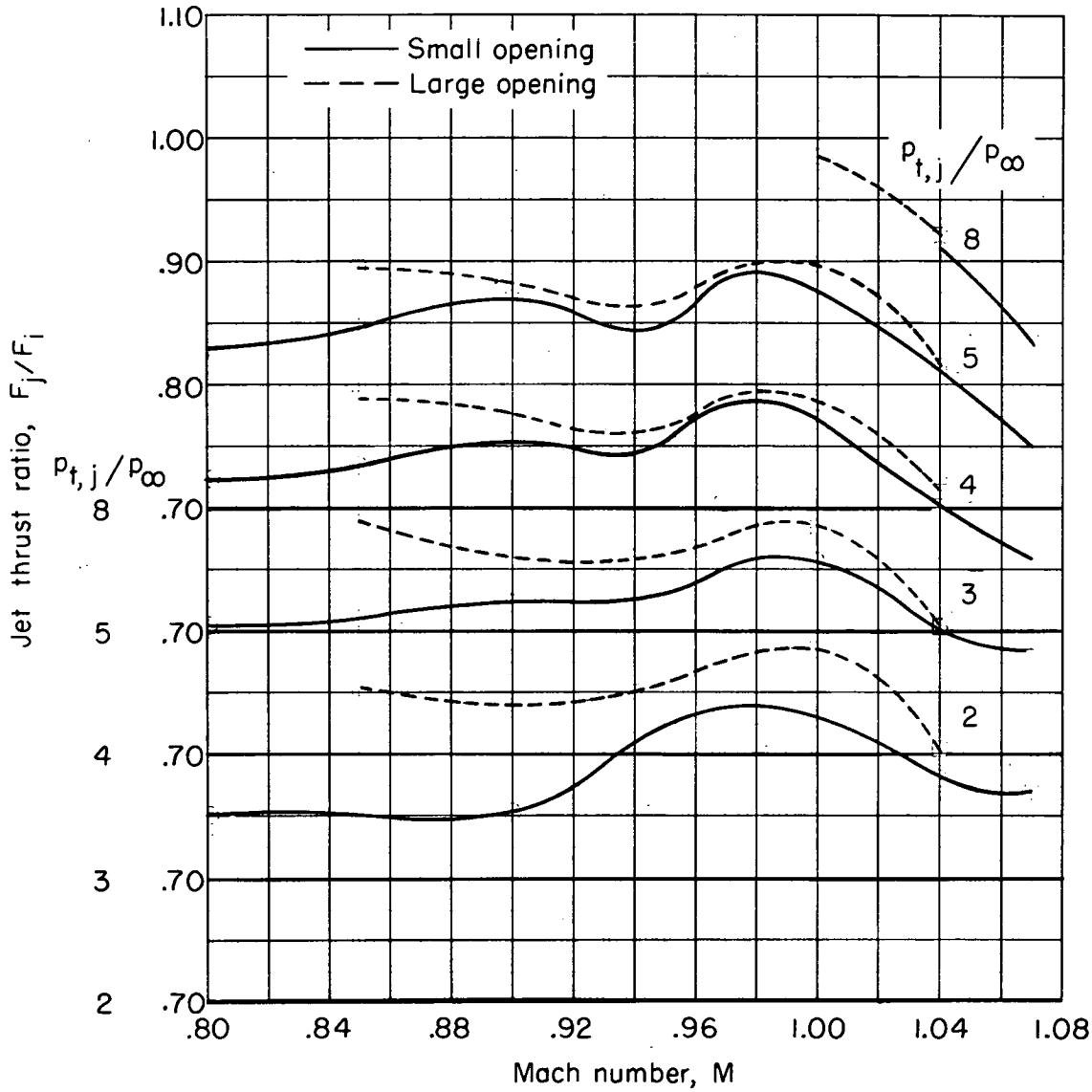

Figure 12.- Variation of jet thrust ratio with Mach number for constant jet pressure ratios.

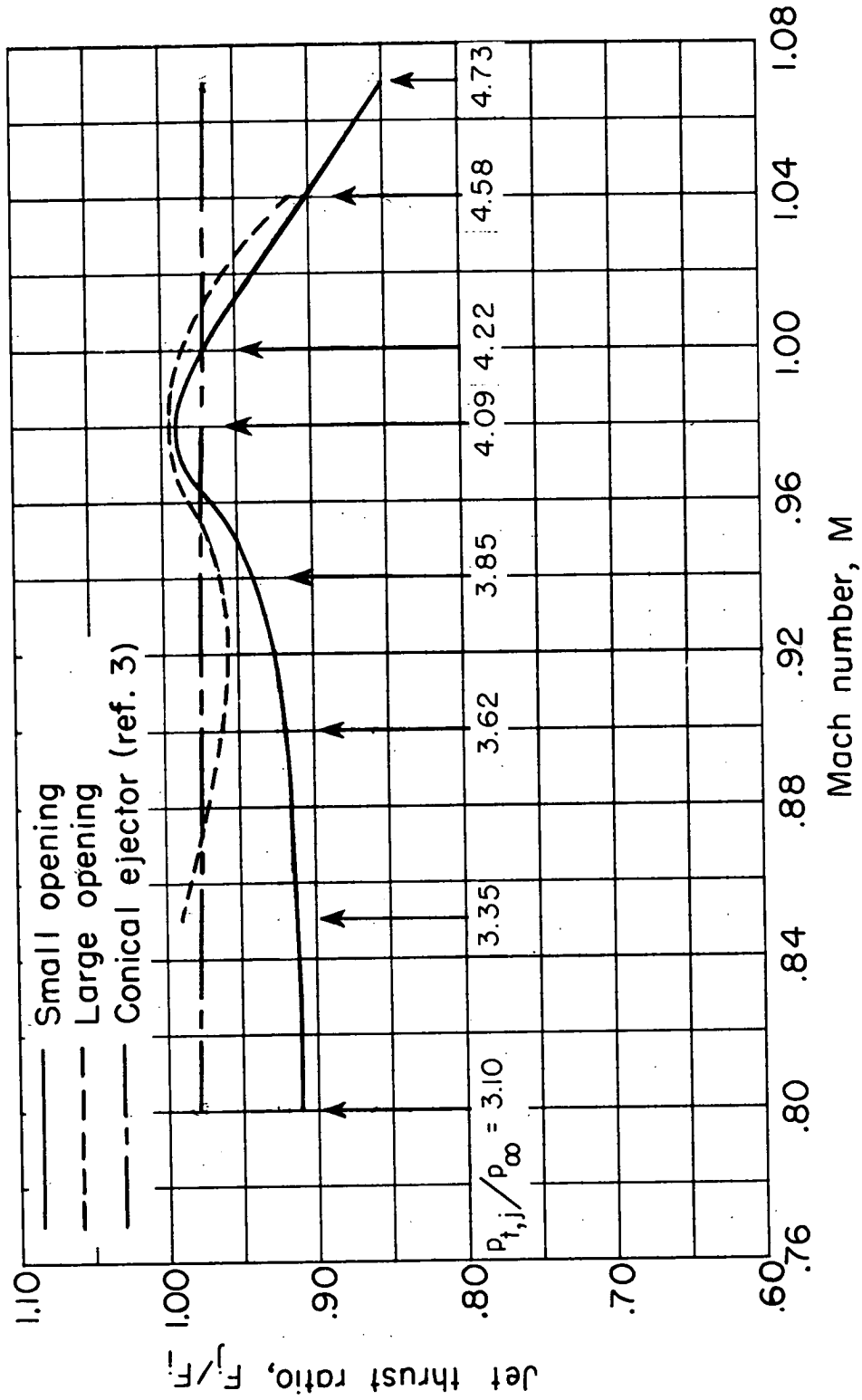

Figure 13.- Variation of jet thrust ratio with Mach number for a typical jet engine pressure ratio schedule and comparison with conical ejector.